REVIEW

Check for updates

Journal of
Sensor Science and Technology

The Korean Sensors Society

Emerging Sensing Strategies for Environmental Micro- and Nanoplastics Detection

Seung Yun Kim[1,*], Rubeen Park[1,*], and Geumbee Lee[1,+]

[1]*School of Chemical Engineering and Applied Chemistry, Kyungpook National University, 80 Daehak-ro, Buk-gu, Daegu, 41566, Republic of Korea*

Cite This: *J. Sens. Sci. Technol. Vol. 35, No. 2 (2026) 148-163*

https://doi.org/10.46670/JSST.2026.35.2.148

ABSTRACT: Micro- and nanoplastics represent a pervasive class of anthropogenic contaminants that originate from the widespread production, use, and degradation of polymeric materials. These particles persist across marine, freshwater, terrestrial, and atmospheric environments and increasingly threaten ecosystems and human health. Reliable detection of micro- and nanoplastics remains challenging because of their small size, low abundance, and chemical heterogeneity. This review summarizes recent advances in sensing strategies that target environmental micro- and nanoplastics, with emphasis on platform-level detection interfaces. The discussion begins with an overview of vibrational spectroscopic techniques, including Raman spectroscopy, surface-enhanced Raman scattering (SERS), and Fourier-transform infrared (FTIR) spectroscopy. Subsequent sections examine electrochemical impedance spectroscopy (EIS) and fluorescence-based sensing approaches. For each strategy, the review discusses detection mechanisms, performance characteristics, and practical constraints in complex environmental matrices. The review further highlights integrated and portable sensing platforms that support *in situ* and real-time analysis. Emerging frameworks that combine sensing interfaces with machine learning–based data analysis receive particular attention for their ability to enhance classification accuracy and robustness. The concluding section outlines current capabilities and identifies opportunities for the development of next-generation sensing platforms for environmental micro- and nanoplastics.

KEYWORDS: *Microplastics detection, Nanoplastics detection, Environmental sensors, Machine learning*

1. INTRODUCTION

Microplastic pollution represents a growing environmental challenge driven by the global increase in plastic consumption. Microplastics generally refer to plastic particles with diameters ranging from 1 μm to 5 mm, while plastics smaller than 1 μm fall into the nanoplastic regime. Based on their origin, microplastics consist of primary and secondary categories. Primary microplastics originate from intentional manufacturing processes, including cosmetic scrub particles, synthetic fibers, and industrial pellets; secondary microplastics emerge from the fragmentation of larger plastic products through physical forces (*e.g.*, waves, abrasion, and impact), as well as chemical processes (*e.g.*, photooxidative chain scission) [1,2].

The chemical stability and high molecular weight of polymer chains hinder microplastic degradation and drive long-term accumulation in natural environments. Microplastics persist in marine, freshwater, and soil systems and modify microbial communities, ionic distributions, and local pH, thereby affecting plant ecosystems [3]. Aquatic organisms ingest microplastics as food analogues and promote trophic transfer across food chains, leading to ecological disruption. Microplastics penetrate human blood, lung, and placental tissues and induce inflammatory responses through micro-scale damage to digestive and respiratory mucosa, indicating direct risks to human health [4-6].

Reliable detection of microplastics in complex natural environments remains a central challenge for environmental monitoring and risk assessment. Conventional analytical techniques face practical limitations, such as extensive sample pretreatment, long acquisition times, and high-cost instrumentation. Portable sensing platforms combined with rapid data processing enable on-site analysis and partially overcome these limitations. However, most existing approaches target a narrow range of polymer types and lack sufficient validation in

*These authors contributed equally to this work.
+Corresponding author: geumbee.lee@knu.ac.kr
Received : Dec. 30, 2025, Revised : Jan. 9, 2026, Accepted : Feb. 21, 2026

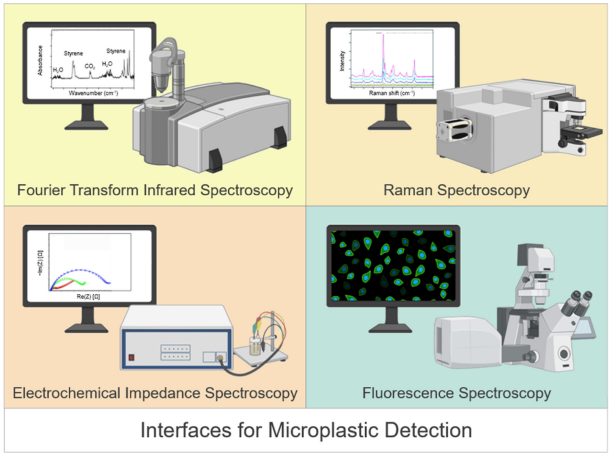

Fig. 1. Schematic illustration of representative interfaces for microplastic detection.

solid-state samples and heterogeneous natural matrices.

This review summarizes recent diverse technologies and tools for microplastic detection and sensing interfaces (Fig. 1). The discussion introduces Raman spectroscopy, surface-enhanced Raman scattering (SERS), Fourier-transform infrared (FTIR) spectroscopy, electrochemical impedance spectroscopy (EIS), and fluorescence-based sensing schemes. Each scheme covers its detection mechanism, advantages, limitations, and applications. The concluding section identifies platform-level opportunities for next-generation micro/nanoplastic sensors, including emerging approaches that integrate machine learning–enabled data analysis.

2. SENSING INTERFACES FOR MICRO- AND NANOPLASTICS DETECTION

This review begins with an overview of representative interfaces in state-of-the-art micro- and nanoplastics sensing, covering Raman spectroscopy, surface-enhanced Raman scattering (SERS), Fourier-transform infrared (FTIR) spectroscopy, electrochemical impedance spectroscopy (EIS), and fluorescence-based approaches.

2.1 Raman Spectroscopy

Raman spectroscopy probes light–matter interactions under laser excitation to analyze molecular structure, composition, and chemical bonding. The technique enables direct analysis of samples without physical state changes or chemical surface treatment. This feature simplifies experimental procedures and supports rapid analysis. Raman spectroscopy operates in a nondestructive manner and preserves the physicochemical properties of the sample. The method applies to solid, liquid, and gaseous samples. These characteristics enable the detection of microplastic-derived materials and contribute to the advancement of microplastic analysis [7].

Low microplastic concentration (< 0.1 wt%) and small particle size (< 1 μm) limit the sensitivity of Raman-based analysis. Low concentrations significantly weaken Raman signal intensity [8]. Furthermore, small particles further reduce signal strength and complicate spectral acquisition [9]. Samples containing multiple microplastic species or coexisting non-plastic materials interfere with the isolation of distinct spectral signatures.

2.1.1 Sensing Mechanism

Raman spectroscopy relies on inelastic scattering, which occurs when laser light interacts with matter. Such scattering is classified into elastic and inelastic processes. Elastic scattering involves no energy change before and after the interaction between light and matter. Inelastic scattering involves energy transfer during the interaction. Raman scattering represents a form of inelastic scattering and includes Stokes scattering, in which a portion of photon energy converts into molecular vibrational energy, and anti-Stokes scattering, in which molecular vibrational energy transfers to photon energy [10].

Raman shift expresses this energy difference as characteristic Raman peaks in wavenumber units (cm^{-1}). Each Raman shift corresponds to a specific molecular vibrational mode and enables identification of molecular structures and functional groups (*e.g.*, C–H, C–C, C=C, etc.). Raman spectroscopy exhibits high sensitivity to changes in molecular polarizability and performs effectively for symmetric, nonpolar covalent bonds. Polar bonds also produce Raman signals, but strongly polar bonds respond more sensitively in FTIR spectroscopy. Raman spectroscopy shows minimal interference from water and supports analysis of solution-phase samples.

Distinct Raman fingerprints enable discrimination of polymer-specific microplastics. Common polymers exhibit characteristic Raman peaks, including Nylon (1631 cm^{-1}), polyethylene terephthalate (PET; 1615 cm^{-1}), polystyrene (PS; 1603 cm^{-1}), polypropylene (PP; 1465 cm^{-1}), and polyethylene (PE; 1294 cm^{-1}), which supports effective identification of diverse microplastic types [11,12].

2.1.2 Recent Examples

Portable Raman spectrometers enable the detection of microplastics in aqueous environments outside laboratory settings and complement conventional benchtop Raman systems (Fig. 2(a)) [13]. These portable systems support real-time measurements through Wi-Fi and Bluetooth communication interfaces and detect low concentrations of microplastics (PS; 8.47 μm in diameter; 0.015-0.075% w/v in concentration). Increasing microplastic content instead attenuates Raman signal

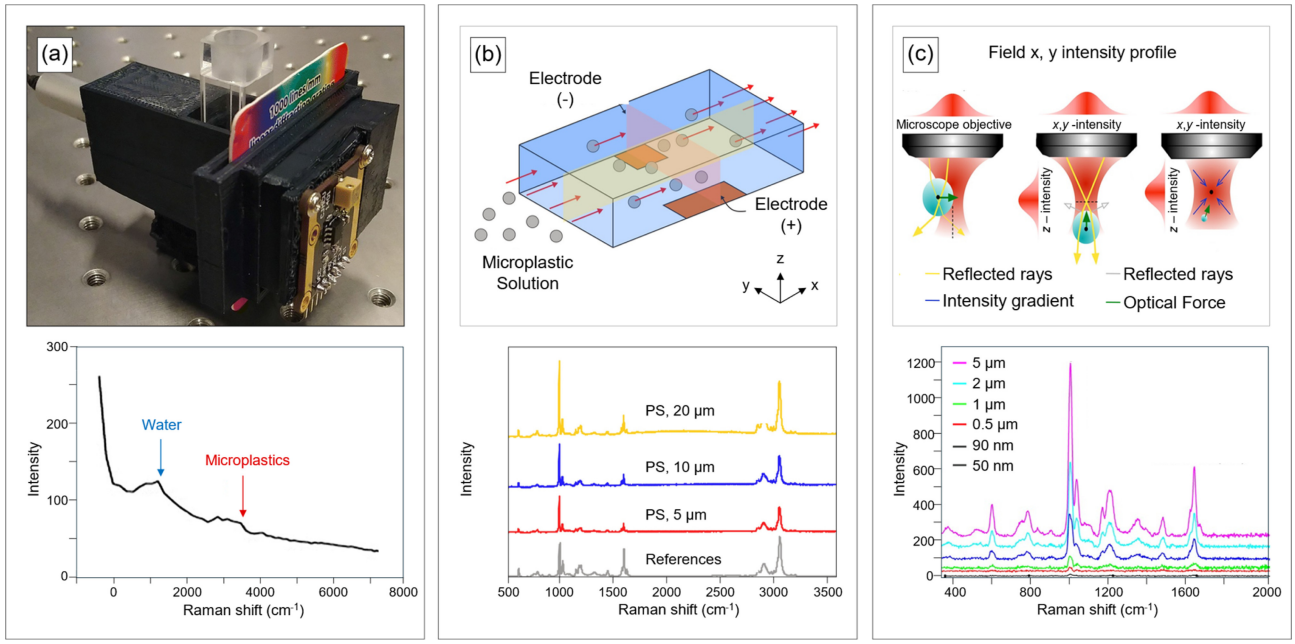

Fig. 2. Interfaces of Raman spectroscopy for microplastic detection. (a) (top) Image of portable, prototype Raman spectrometer with a three-dimensional printed case. (bottom) Raman spectra of microplastics solution. Blue arrow: de-ionized water; red arrow: microplastics (PS; concentration : 0.075% w/v). Adapted from Ref. [13]. (b) (top) Illustration of the microplastic capture mechanism by electrophoresis in a microchannel. (bottom) Raman spectra of PS with various sizes captured using electrophoretic removal method. Adapted from Ref. [16]. (c) (top) Working principle of Raman tweezers. (bottom) Raman spectra of concentration-dependent PS (concentration: 5.68×10^{9}-3.64×10^{14} particles·mL^{-1}). Adapted from Ref. [17].

intensity due to light blocking within the sample. The system operates at a fabrication cost below $370, substantially lower than the average cost of commercial Raman instruments (> $15,000). Its compact device size (5.6 cm×5.6 cm×3.1 cm) and high portability facilitate deployment in rivers, lakes, and marine environments for real-time monitoring applications [14,15].

Electrophoretic separation provides an alternative strategy for isolating microplastics in fluidic environments based on surface charge characteristics (Fig. 2(b)) [16]. Most microplastics possess negatively charged surfaces and migrate toward the anode under an applied electric field. A straight microfluidic channel with embedded electrodes (1.5 cm×6 cm) captures microplastics (PS; 5 μm in diameter; 1.5×10^{3} particles×mL^{-1} in concentration) with up to ~79% efficiency under a DC electric field (10 V) and a controlled flow rate (5 mL×h^{-1}). Increased flow rates reduce capture efficiency under identical electric field conditions. A loop-based recirculation system restores capture performance and increases efficiency from ~30% to 62% with a single injection. This approach enables microplastic collection from tea bag-based environmental samples and supports *in situ* Raman analysis without additional pretreatment.

Raman tweezers (RT) integrate Raman spectroscopy with optical tweezers to enable single-particle trapping and analysis (Fig. 2(c)) [17]. RT analyzes a broad range of microplastic compositions (*e.g.*, PP, PS, PE, PET, polyvinyl alcohol [PVA], polymethyl methacrylate [PMMA], polyamide-6 [PA6]), particle sizes (0.05-20 μm in diameter), and morphologies in distilled water and seawater. Optical trapping arises from momentum changes during photon reflection and refraction when the particle size exceeds the incident wavelength. The numerical aperture (NA) of the focusing optics governs trapping stability. In contrast, particles much smaller than the incident wavelength experience induced dipole formation under an external electric field. These dipolar microplastic particles migrate toward the laser focal point under the electromagnetic field.

2.2 Surface-Enhanced Raman Scattering

Surface-enhanced Raman scattering (SERS) extends Raman spectroscopy to overcome its sensitivity limitations. Raman spectroscopy probes molecular vibrational modes through inelastic light scattering and provides chemical information. Raman signals remain inherently weak and limit analysis of low-concentration species (< 0.1 wt%) and small particles (< 1 μm). SERS addresses these limitations by introducing metallic, nanostructured surfaces (*e.g.*, gold and silver). Optical excitation of these nanostructures induces localized surface plasmon resonance and generates intense electromagnetic fields near the metal surface [18]. These localized fields

strongly amplify Raman scattering from nearby molecules. Signal enhancement factors reach up to ~10^8 relative to conventional Raman spectroscopy. This amplification enables detection of trace-level analytes and supports single-molecule detection under favorable conditions.

The performance of SERS depends strongly on the geometry, size, spacing, and arrangement of metallic nanostructures. Variations in substrate structure and measurement position introduce signal fluctuations and reduce reproducibility. The intensity of the Raman signal also depends on molecular proximity and adsorption behavior at the metal surface, which limits quantitative analysis. SERS-based plastic detection, thus, requires consistent substrate design and well-defined measurement conditions.

2.2.1 Sensing Mechanism

SERS involves two enhancement mechanisms: electromagnetic enhancement (EM) and chemical enhancement (CE) [19,20]. EM arises when incident light excites collective oscillations of free electrons in metallic nanostructures, inducing localized surface plasmon resonance (LSPR). The LSPR effect generates intense localized electromagnetic fields near the metal surface. These fields strongly amplify Raman scattering from plastic molecules located within the enhanced field region. EM typically yields enhancement factors ranging from several thousand to several million and reaches higher amplification levels (on the order of 10^5-10^9) than CE [21]. EM amplifies Raman signals in a largely nonselective manner, whereas CE selectively enhances specific Raman peaks associated with molecular electronic structure and vibrational modes. CE originates from charge transfer interactions between the metal surface and plastic molecules. Chemical adsorption of plastic molecules onto the metal surface establishes energetically allowed electron transfer pathways between the metal Fermi level and molecular orbitals. Depending on energy-level alignment, electrons transfer from the metal to the molecular lowest unoccupied molecular orbital (LUMO) or from the molecular highest occupied molecular orbital (HOMO) to the metal. These interactions modify the electrical polarization and polarizability of plastic molecules, increase Raman scattering probability, and enhance detection sensitivity [22].

2.2.2 Recent Examples

Under flow conditions within the sample, microplastics associate with gold nanorods (GNRs), inducing strong plasmonic resonance that amplifies SERS signals [23]. A 785 nm-laser matches the longitudinal plasmon resonance of GNRs and maximizes optical absorption (Fig. 3(a)). Absorbed optical energy converts into heat and generates localized photothermal heating around the GNRs. A temperature

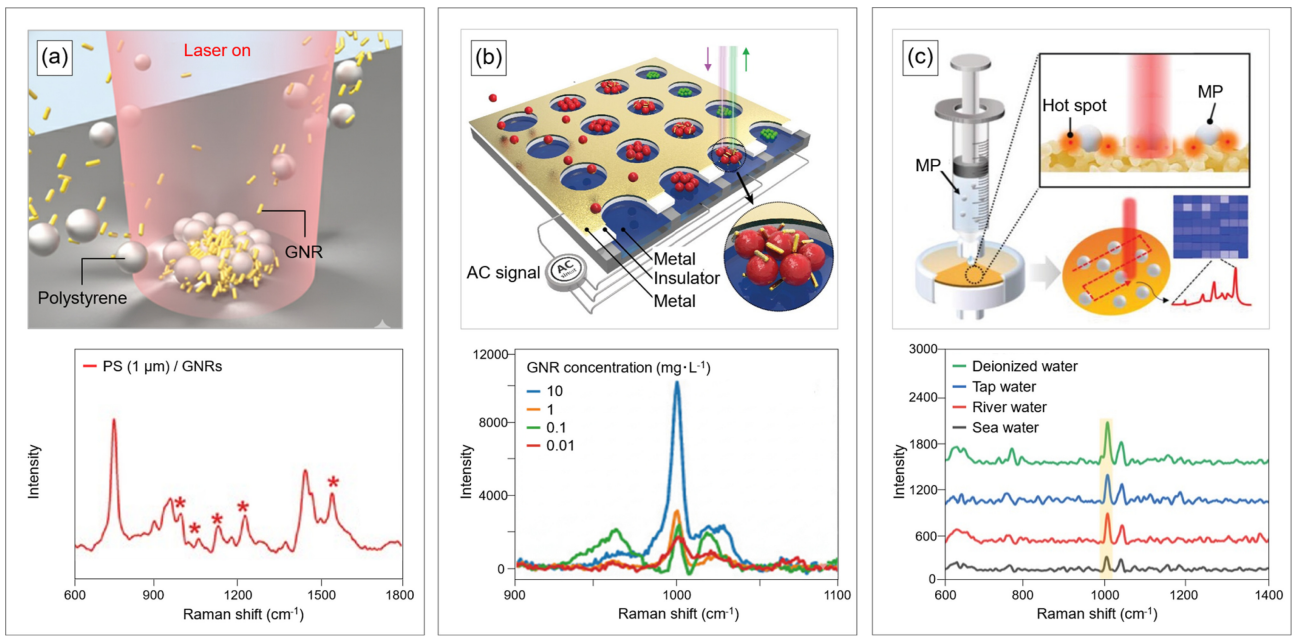

Fig. 3. Interfaces of SERS for microplastic detection. (a) (top) Schematic illustration of PS detection utilizing photothermal convection of gold Nanorods (GNRs; concentration: 7.0×10^{11} particles·mL^{-1}). (bottom) Raman spectra of PS obtained under GNR-assisted 3D co-assembly, Adapted from Ref. [23]. (b) (top) Conceptual diagram of the DEP-ACEO-Raman-tweezer (DART) substrate for real-time, on-site Raman detection of nanoplastic. (bottom) Raman spectra of PS (diameter: 200 nm) at various concentration GNRs from 10 mg·L^{-1} to 0.01 mg·L^{-1}. Adapted from Ref. [24]. (c) (top) Schematic illustration of a SERS-ML-based in-situ MP detection device. (bottom) Average Raman spectra of PS (diameter: 1 μm, concentration: 100 μg·mL^{-1}) spiked into various environmental samples (deionized water, tap water, river and seawater). Adapted from Ref. [26].

gradient between the laser focus and the surrounding solution drives photothermal convection within the sample. This flow transports GNRs and nanoplastic particles (*i.e.*, PS) of various sizes (100 nm, 500 nm, and 1 μm) toward the laser focus and promotes formation of three-dimensional co-assembly structures. Such photothermal convection–driven, three-dimensional (3D) co-assembly amplifies Raman signals from microplastics by up to fourfold and extends the detection range to microplastic concentrations as low as 1 ppm.

As an alternative approach, the application of an alternating electric field to an aqueous medium induces the active transport of nanoplastics and forms high-density electric clustering of PS (30-200 nm in diameter) and GNRs [24] (Fig. 3(b)). In a nonuniform electric field, differences in dielectric properties generate dielectrophoretic (DEP) forces, while ions in the electric double layer at the electrode surface interact with the tangential component of the electric field to produce AC electro-osmotic (ACEO) flow. The combination of DEP and ACEO drives electric-field-based trapping and focusing of particles. The resulting clustered structures enhance Raman signal sensitivity and expand detection to trace-level nanoplastics (PS; 30 nm in diameter; 10 $\mu g \times L^{-1}$) comparable to concentrations reported in seawater (average concentration: ≈20 $\mu g \times L^{-1}$) [25].

3D plasmonic gold nanopockets (3D-PGNPs) serve as porous, SERS-active substrates that enable simultaneous microplastic capture and Raman signal amplification (Fig. 3(c)) [26]. 3D-PGNPs form through solution-based synthesis on cellulose acetate filters and generate strong volumetric plasmonic hotspots at microplastic interfaces. Integration of 3D-PGNP substrates with syringe filter devices captures both PS (1 μm in size; 10-1000 $\mu g \times mL^{-1}$) and PE (1-4 μm in size; 50-1000 $\mu g \times mL^{-1}$) efficiently. Raman mapping visualizes the spatial distributions of captured microplastics, and a logistic regression-based machine learning model classifies particle distributions as positive or negative. This approach demonstrates the identification of microplastics in real tap water, river water, and seawater samples.

2.3 Fourier-Transform Infrared Spectroscopy

Fourier-transform infrared (FTIR) spectroscopy identifies molecular structures by measuring absorption signals associated with vibrational and rotational modes under mid-infrared irradiation (2.5-25 μm in wavelength). Each chemical bond exhibits characteristic vibrational energies, and FTIR captures material-specific spectral fingerprints through wavelength-dependent absorption intensity. Most molecules absorb infrared radiation, which enables FTIR analysis of solid, liquid, and gaseous samples. The technique offers simple sample preparation and nondestructive analysis. FTIR supports multiple operational modes, including transmission, attenuated total reflection (ATR), diffuse reflectance infrared Fourier transform (DRIFT), and micro-FTIR. Environmental microplastics exhibit broad variation in size, morphology, transparency, and surface contamination. Appropriate selection of the FTIR mode remains essential for reliable analysis [27].

Both FTIR and Raman spectroscopy provide nondestructive analysis but rely on different sensitivity in mechanisms. FTIR responds to changes in molecular charge distribution and favors polar bonds (*e.g.*, C=O, O–H); Raman spectroscopy responds to changes in molecular polarizability and favors nonpolar bonds (*e.g.*, C–C, C=C). FTIR performs effectively for particles with diameters larger than 20 μm, while Raman spectroscopy supports analysis of particles smaller than 1 μm. The complementary use of these two techniques improves chemical identification across diverse bonding types and particle sizes [28].

Low analyte concentration and small particle size constrain the analytical performance of FTIR spectroscopy. Low sample concentrations (< 0.1 $mg \times L^{-}$) and small particle sizes (< 20 μm) reduce detection reliability [29,30]. Infrared–particle interactions involve both absorption and scattering. Scattering behavior follows Rayleigh scattering (*i.e.*, particle size < wavelength), Mie scattering (*i.e.*, particle size ≈ wavelength), and geometric optical scattering (*i.e.*, particle size > wavelength). The average size of environmental microplastics often matches mid-infrared wavelengths, which promotes dominant Mie scattering. Mie scattering induces diffraction, reflection, refraction, and absorption effects that distort infrared spectra [31]. In addition, water exhibits strong absorption bands (O–H: 3000–3500 cm^{-1}; H–O–H: ~1600 cm^{-1}). As a result, these bands interfere with the FTIR analysis of microplastics in aqueous environments (*e.g.*, seawater or freshwater systems) and require careful interpretation [32].

2.3.1 Sensing Mechanism

The horizontal axis (*i.e.*, *x*-axis) of an FTIR spectrum represents the wavenumber (cm^{-1}), defined as the inverse of wavelength, while the vertical axis (*i.e.*, *y*-axis) represents absorbance and reflects the intensity of absorbed light at characteristic frequencies. FTIR detects functional groups present in polymeric microplastics, including PS, PP, PE, and PET. Chemical bonds along polymer chains exhibit characteristic absorption bands at specific wavenumber regions, such as C=O (1700–1750 cm^{-1}), O–H (3200–3600 cm^{-1}), and C–H (2800–3000 cm^{-1}) [33]. These spectral features enable discrimination of microplastics through functional group identification. The absorbance intensity follows the Beer-Lambert law (absorbance ∝ concentration) and supports quantitative analysis of microplastic concentration [34].

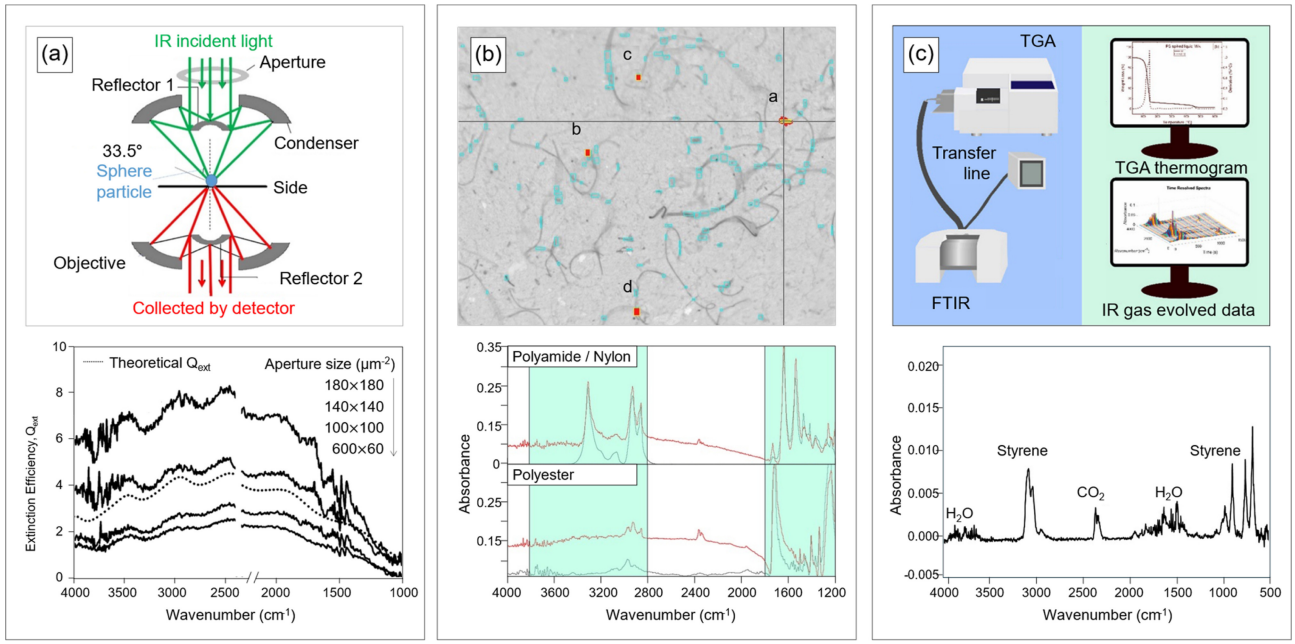

Fig. 4. Interfaces of FTIR for microplastic detection. (a) (top) Schematic illustration of the transmission mode used in micro-FTIR spectroscopy. (bottom) FTIR spectra of PS measured with different aperture sizes (solid lines: measured data; dash lines: theoretical data). Adapted from Ref. [35]. (b) (top) Optical screenshot at the detecting point. (bottom) Micro-FTIR spectra of polyamide/nylon and polyester (diameter: 1-500 μm). Adapted from Ref. [36]. (c) (top) Schematic illustration of the experimental setup for TGA-FTIR and data acquisition. (bottom) Gas-phase FTIR spectra of PS (concentration: 33.94 μg·mL^{-1}) released in water. Adapted from Ref. [40].

2.3.2 Recent Examples

Understanding the origin and extent of spectral distortion improves the reliability of FTIR-based microplastic detection. Mie scattering strongly depends on experimental conditions, including the fraction of scattered light, aperture size, and optical throughput. A high fraction of scattered light redirects unabsorbed photons away from the detector, thereby reducing analytical reliability.

Aperture size defines the spatial range of collected light, while optical throughput represents the ratio of detected light to incident light and reflects optical loss and scattering severity. Quantitative control of scattered light fraction, aperture size, and optical throughput therefore remains essential for accurate FTIR analysis. Fig. 4(a) presents microplastic detection using micro-FTIR that integrates an optical microscope lens with FTIR to evaluate scattering behavior as a function of aperture size. The analysis detects microplastics (PS; 4.46 μm in diameter) and shows increasing spectral distortion with larger aperture sizes due to an elevated fraction of scattered light [35].

Most FTIR-based microplastic studies rely on controlled laboratory conditions. Practical analysis under realistic environmental conditions requires further investigation. For example, Fig. 4(b) illustrates the detection of synthetic fibers, defined as microplastics, in laundry wastewater generated from household towel washing. FTIR identifies PE (≈500 μm in size) and polyamide (PA; ≈500 μm in size) across a range of particle sizes after purification removes residual detergents from the wash water [36]. FTIR spectroscopy also characterized microplastics collected from surface seawater in the Ross Sea, Antarctica. Filtration of seawater samples (volume: ≥2000 L) through stainless-steel sieve (250 μm in pore size) enables analysis of the presence and characteristics of microplastics (PE and PP: 0.14-4.99 mm in size) [37].

Microplastic detection in food matrices presents greater complexity than analysis in aqueous systems. Food matrices contain lipids, proteins, organic matter, and pigments that act as interfering components and degrade the precision of FTIR spectral signals. The combination of thermogravimetric analysis (TGA) with FTIR provides an alternative strategy to address limitations associated with conventional FTIR-based microplastic detection. TGA monitors mass changes as a function of temperature under controlled heating conditions and evaluates thermal decomposition behavior. The integrated TGA–FTIR approach represents a relatively recent analytical technique. Standardized protocols remain limited, but the method shows strong potential for microplastic analysis in complex matrices, including food and cosmetic samples [38,39]. For instance, TGA–FTIR enables identification and quantification of microplastics across diverse liquid and environmental samples (Fig. 4(c)). The technique detects PS (1 μm in diameter) in beverages (*e.g.*, water, including liquid skimmed milk and ground coffee). The approach also

identifies polyvinyl chloride (PVC; < 5 mm in size) and PS (< 125 μm in size) in environmental samples (mussel tissue, seawater, and soil) [40]. Multivariate regression analysis, including partial least squares methods, reduces food matrix interference and enables quantitative estimation of microplastic concentration based on FTIR-derived evolved gas data [41].

Pyrolysis-based analytical techniques provide an additional thermal analysis strategy [42]. Pyrolysis-gas chromatography–mass spectrometry rapidly decomposes complex environmental samples, including soil and biological tissues, under high-temperature conditions and performs mass spectrometric analysis of decomposition products. This approach even supports identification of nanoplastics (PS, < 900 nm in size; PP, < 1000 nm in size).

2.4 Electrochemical Impedance Spectroscopy

Impedance (Z) describes resistance in an alternating current (AC) circuit and follows the mathematical expression:

$$Z = \mathrm{Re}(Z) + j\mathrm{Im}(Z)$$

The real part (*i.e.*, Re(Z)) represents the resistive component, and the imaginary part (*i.e.*, Im(Z)) represents the reactive component, where j denotes the imaginary unit. Unlike resistance in direct current circuits, impedance appears as a complex quantity that includes both magnitude and phase. Electrochemical impedance spectroscopy (EIS) in electrochemical systems follows the expression:

$$Z = R_s + \frac{1}{j\omega C_{\mathrm{dl}}} + R_{\mathrm{ct}} + Z_{\mathrm{w}}$$

This representation models physical processes at the electrode–electrolyte interface using discrete circuit elements. The solution resistance, R_s, reflects the intrinsic resistance of the electrolyte. The double-layer capacitance, $\frac{1}{j\omega C_{\mathrm{dl}}}$, accounts for charge separation at the interface. The charge-transfer resistance, R_{ct}, describes resistance associated with electron transfer across the interface. The Warburg impedance, Z_{w}, represents diffusion-controlled resistance related to ion transport [43,44].

EIS applies a small-amplitude AC signal between electrodes and measures the resulting response to determine impedance. The presence, type, and amount of material between electrodes modify the impedance response. Resulting changes in impedance enable estimation of both material identity and quantity within the system. EIS offers low cost, simple operation, and effective performance across a wide range of applications, including batteries [45,46], disease diagnostics [47,48], and environmental sensors [49,50]. The technique supports facile *in situ* measurements and serves as a platform for microplastic detection [51-53].

2.4.1 Sensing Mechanism

Microplastic detection using EIS relies on the measurement of impedance changes associated with the presence and concentration of particles [54,55]. The adsorption of microplastics onto the electrode surface alters the electrode–electrolyte interfacial structure and restricts charge-transfer pathways, resulting in increases the R_{ct} [54]. This increase directly affects the overall impedance value. Higher microplastic concentrations promote greater particle adsorption on the electrode surface, facilitating a corresponding increase in impedance [56].

2.4.2 Recent Examples

EIS-based microplastic detection primarily targets microplastics suspended in liquid samples by measuring impedance differences that vary with microplastic concentration. The method introduces microplastic samples between electrodes through drop casting or continuous flow and records impedance responses during sample passage. One representative system arranges gold-plated circuit boards in a parallel configuration to form paired electrodes (Fig. 5(a)) [57]. A gravity-driven flow containing PE beads (212-1000 μm in size) and mixed biological specimens passes between the electrodes. The system applies AC voltages across a range of frequencies and measures the resulting current response. Low-frequency signals provide information related to particle volume, while high-frequency signals probe internal particle properties. The analysis classifies particles using a k-nearest neighbors (k-NN) algorithm based on impedance features. The study compares classification reliability using a 12-dimensional k-NN model that incorporates Re(Z) and Im(Z) values at 6 frequencies and a 2-dimensional k-NN model that uses impedance magnitude changes at two frequencies. The platform distinguishes microplastics, organisms, and bubbles by assigning weighted similarity scores relative to reference impedance datasets.

An alternative strategy employs microrobots that directly capture microplastics rather than relying on flow-based sensing [58]. The microrobots consist of titanium dioxide (TiO_2)–derived MXene coated with a platinum (Pt) layer (50 nm in thickness) and embedded with maghemite nanoparticles (γ-Fe_2O_3; < 50 nm in size) (Fig. 5(b)). Ultraviolet (UV) irradiation of the Pt/TiO_2 layer excites electrons due to the TiO_2 bandgap energy (*i.e.*, 3.8 eV) and generates protons. Electrons migrate to the Pt surface and form hydrogen gas. The resulting gas concentration gradient generates a driving force that propels the microrobots. Positively charged microrobots capture

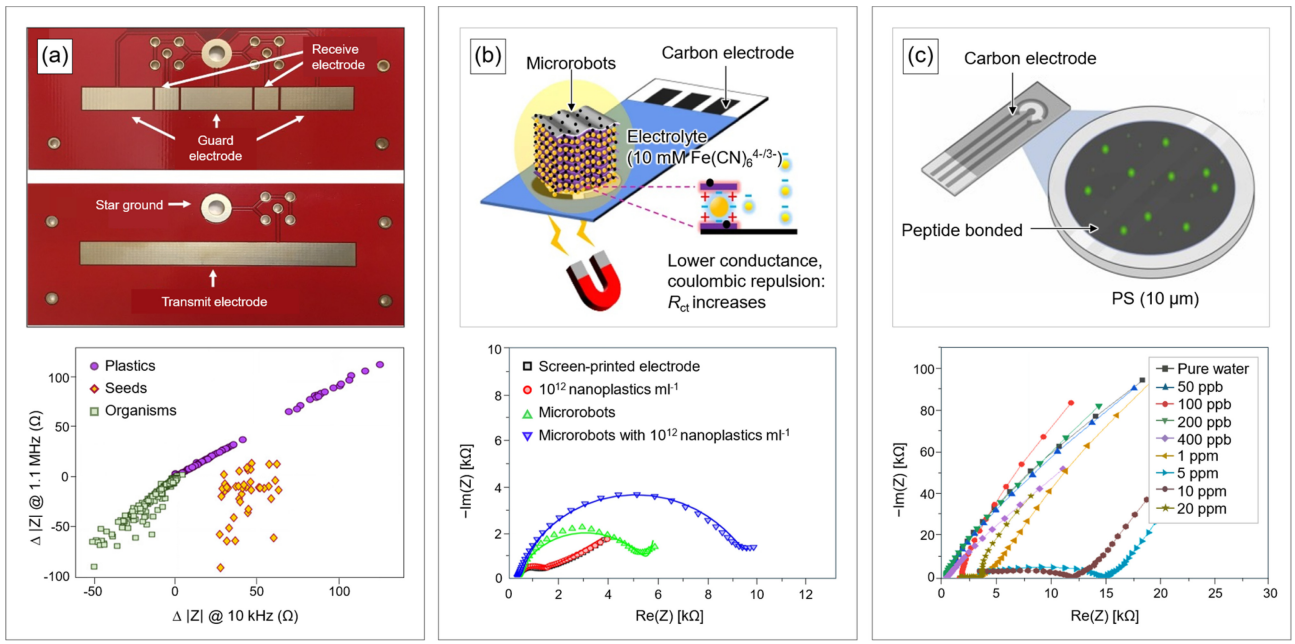

Fig. 5. Interfaces of EIS for microplastic detection. (a) (top) Gold-plated circuit boards used for impedance measurements. (bottom) Changes in impedance of plastic samples, seeds and organisms (measured frequency: 10 kHz and 1.1 MHz). Adapted from Ref. [57]. (b) (top) Screen-printed, carbon electrode with MXene ($Ti_3C_2T_x$)-derived microrobots. (bottom) Changes in Nyquist plots of multiple substrates (measured frequency: 10^0 to 10^5 Hz). Adapted from Ref. [58]. (c) (top) Sensor setup based on a Peptide (Ahx-MPAVMSSAQVPR)-coated carbon electrode. (bottom) Changes in Nyquist plots of PS particles at different concentration (measured frequency: 0.1 to 1 MHz). Adapted from Ref. [52].

negatively charged microplastics through electrostatic attraction and allow magnetic recovery through γ-Fe_2O_3-derived magnetism. A screen-printed three-electrode system with a working (carbon), a counter (carbon) and a reference electrode (Ag/AgCl), measures impedance changes associated with microplastic capture.

Peptide-functionalized impedance sensors provide another route for microplastic detection (Fig. 5(c)). Peptides (*e.g.*, amino acids) coat screen-printed carbon electrodes and interact selectively with PS beads (2–250 μm in size). Hydrophobic PS beads interact preferentially with hydrophobic amino acids such as methionine and proline. Negatively charged polar PS binds to charged amino acids such as arginine. This interaction mechanism enables peptide-based impedance sensors to achieve low limits of detection (*e.g.*, 50 ppb in deionized and tap water; 400 ppb in seawater) [52].

Additional approaches employ extracellular polymeric substances extracted from cyanobacteria as membrane materials [59]. Functional groups on the membrane surface (*e.g.*, sulfate [–SO_4^{2-}], hydroxyl [–OH], and carboxyl [–COOH] groups) bind microplastics through London dispersion forces, electrostatic attraction, and hydrogen bonding. These interactions induce measurable impedance changes and support microplastic detection. Another strategy fabricates graphene electrodes with honeycomb architectures to increase surface area and promote physical adsorption, enabling measurements of microplastic concentration (*e.g.*, PS; 0.08-20 μm in size) [56].

Overall, EIS-based approaches detect microplastics by sensing impedance changes that arise from physical and chemical interactions. The technique provides rapid and straightforward identification of microplastic presence and concentration. Low cost and compatibility with *in situ* measurements further support the potential of EIS platforms for future microplastic monitoring applications.

2.5 Fluorescence

Conventional detection methods based on optical microscopy rely on visual inspection of microplastics after removal of large particles and non-target organic matter from samples. This approach offers rapid and simple analysis, but suffers from limited reliability. In addition, the method shows reduced sensitivity toward small particles (< 1 mm) and optically transparent plastics with a risk of misidentification [60,61]. This section introduces fluorescence-based strategies that address these limitations by labeling particles with fluorescent probes and detecting light emitted from the probes.

Fluorescence arises when specific molecules absorb incident light and transition to an excited energy state, followed by emission of lower-energy light during relaxation to the ground

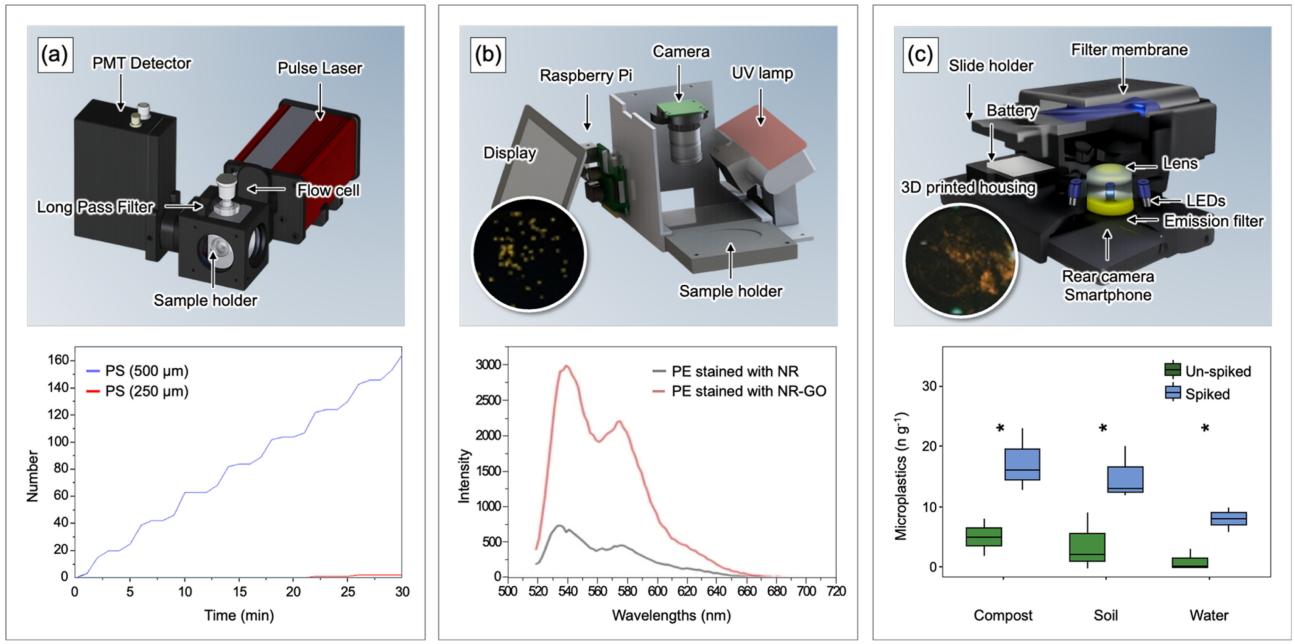

Fig. 6. Interfaces of fluorescence for microplastic detection. (a) (top) Structure and configuration of an optical sensor for detection using pulsed laser excitation and photomultiplier tube (PMT) detector. (bottom) Sensing data from the microplastic monitoring system in real-time. Adapted from Ref. [71]. (b) (top) Schematic illustration of a sensor system designed for portable monitoring of microplastics in water, based on UV LED (wavelength: 254 nm). (bottom) Fluorescence intensity of NR and NR-GO-stained PE. Adapted from Ref. [72]. (c) (top) Three-dimensional rendering of an attachment for an opto-mechanical smartphone. (bottom) Microplastic concentrations measured in spiked (*i.e.*, microplastic-added) and non-spiked (*i.e.*, natural) samples. Adapted from Ref. [73].

state. Absorption of external light promotes electrons to higher energy levels within the molecule. Partial energy dissipation occurs through nonradiative pathways such as heat release. Subsequent photon emission stabilizes the molecule in the ground state. Energy loss prior to emission shifts the emitted light toward longer wavelengths relative to the absorbed light, producing observable fluorescence [62].

2.5.1 Sensing Mechanism

Fluorescence-based detection typically begins with labeling microplastic particle surfaces using fluorescent probes (*e.g.*, Nile Red, fluorescein isothiocyanate, and rhodamine B) [63]. Nile Red (*i.e.*, 9-diethylamino-5-benzo[α]-phenoxazinone), one of the most widely used fluorescent dyes, adsorbs onto microplastics through hydrophobic interactions. This absorbs light in the wavelength range of 450-510 nm (λ_{ex}) and emits fluorescence at 515-590 nm (λ_{em}) [64,65].

Fluorescein isothiocyanate (FITC; λ_{ex}: 450-490 nm; λ_{em}: 510-550 nm) binds to microplastic surfaces through covalent interactions between its isothiocyanate group (–N=C=S) and surface –NH_2 groups present on microplastics [64-66]. Rhodamine B (λ_{ex}: ≈550 nm; λ_{em}: ≈570 nm) typically carries a positive charge and exhibits hydrophobic character. The dye binds to negatively charged microplastics through electrostatic attraction and associates with hydrophobic plastics through hydrophobic interactions [64,67-69].

Direct imaging and fluorescence microscopy analyze and quantify fluorescent signals emitted from selectively labeled microplastics [70]. Fluorescence-based detection offers low cost, rapid staining, and fast signal acquisition. The approach also provides stronger signal intensity than conventional optical microscopy.

2.5.2 Recent Examples

Fluorescence-based detection generally consists of a system that induces and captures fluorescence signals and an analytical module that processes the detected signals. Fig. 6(a) presents a microplastic detection system that operates through sample aspiration [71]. The system integrates a light source and a detector to form an optical sensing unit. Vertical alignment of the optical components enables detection of scattered fluorescence signals. The system analyzes samples through a discontinuous flow sequence that involves repeated aspiration, detection, and release. A communication module transmits fluorescence detection signals via LoRa, enabling remote, real-time monitoring. Experimental measurements using PS beads (500 μm in size) over 30 min record 167 counts – the system correctly identifies 165 particles, with minor errors (*i.e.*, two particles of 250 μm).

Fig. 6(b) illustrates a continuous flow-based detection

platform. The system utilizes a pump for sample aspiration and captures microplastics with a filter (300 μm in pore size) [72]. A camera system detects fluorescence intensity from the filter surface after staining captured microplastics with a Nile Red-graphene oxide (NR-GO) composite. Preparation of NR-GO involves mixing graphene oxide powder with a Nile Red solution. Compared with Nile Red alone, NR-GO provides uniform dispersion on microplastic surfaces and enhances hydrophobic interactions with polymeric materials. This interaction produces stronger fluorescence signals. Emission wavelength analysis reveals color variations that correlate with surface polarity. Nonpolar PE (300 μm in size) and PP (300 μm in size) emit yellow fluorescence (λ_{em} : 560-570 nm). PET (300 μm in size) with strongly polar functional groups (*i.e.*, ester groups; –COO–) emits red–orange fluorescence (λ_{em} : 610-620 nm). PVC (250 μm in size) and PS (900 μm in size) with intermediate surface polarity emit orange fluorescence (λ_{em} : 590-600 nm).

In contrast to pipe- and motor-driven aspiration systems, simplified fluorescence analysis platforms also employ smartphones. A smartphone integrates an external setup that includes a 3D-printed housing, four LEDs, an emission filter, an external lens, and a battery (Fig. 6(c)) [73]. LEDs (450-495 nm in wavelengths) excite fluorescence from NR-stained microplastic surfaces. The smartphone camera images the emitted fluorescence, and analytical algorithms quantify microplastic count and spatial distribution. The system completes analysis within an hour per sample and applies to both artificial samples and real environmental samples.

Fluorescence-based detection also employs pyrene to visualize luminescence from PS beads (2.15, 2.29, and 2.37 μm in size) [74]. Pyrene exhibits polarity-dependent fluorescence behavior and functions as a nonpolar probe. The dye adsorbs onto PS surfaces through hydrophobic interactions and generates strong fluorescence signals. In contrast, pyrene shows weak adsorption and low fluorescence intensity on sand and silica substrates. This selectivity reduces false-positive detection arising from non-plastic materials and improves identification of true microplastic distributions.

Despite these advantages, fluorescence-based sensing presents intrinsic limitations. The approach relies on selective binding of fluorescent probes to specific microplastic types, including Nile Red-PP [75] and fluorescein-PS [65]. In addition, naturally fluorescent microplastics (*e.g.*, PMMA, λ_{em} : 633 nm) and organic compounds (chlorophyll a, λ_{em} : ≈430 nm; phenolic compounds, λ_{em} : 320–370 nm), introduce a risk of misidentification [76]. These constraints highlight the need for further discussion and refinement of fluorescence-based microplastic detection strategies.

2.6 Machine Learning Assisted Detection

Machine learning (ML) techniques effectively handle large-scale data detection and classification and support applications across diverse fields [77,78]. In microplastic research, ML methods organize and classify data obtained from conventional detection techniques and serve as tools to predict microplastic type and concentration. This section summarizes representative examples that integrate ML with previously introduced detection platforms.

One application combines ML with Raman spectroscopy to analyze five types of nanoplastics, including PS and PMMA (spheres; 360 nm, 500 nm, and 1 μm in diameter), PE and polytetrafluoroethylene (PTFE) (pellets; ≤ 1 μm in diameter), and PVC (pellets; 0.3-1 μm in diameter) (Fig. 7(a)) [79]. Nanoplastics generate weak Raman signals and exhibit high noise levels [80]. To address this limitation, the analysis applies a random forest model. The random forest algorithm constructs multiple independent decision trees based on random feature selection and generates predictions through majority voting. The workflow also incorporates a Peak Extraction and Retention (PEER) algorithm to preserve informative peaks and remove noise prior to training. The model assigns weights to characteristic Raman peaks specific to each polymer and classifies microplastics accordingly. Higher weights indicate features that contribute more strongly to classification. Evaluation using unknown samples yields an average accuracy of 98.8%, an average sensitivity of 98.5%, and an average specificity of 100%. In addition to random forest models, one-dimensional convolutional neural networks (1D CNNs) extract features from one-dimensional spectral data and quantify the concentration of PE particles (10, 25, 48, 150, 270, and 500 μm in size) [81]. Other studies apply k-NN models that classify samples based on similarity to reference datasets and distinguish fourteen types of microplastics, including PE, PP, PS, PMMA, PET, PVC, PTFE, polyurethane (PU), acrylonitrile butadiene styrene (ABS), polyoxymethylene (POM), polycarbonate (PC), and silicone [82].

FTIR spectroscopy also generates spectral datasets and supports ML approaches similar to those used for Raman analysis. Convolutional neural networks train on μFTIR datasets (Fig. 7(b)) [83]. Comparative evaluation across different input features and ML models uses the F1-score as a performance metric. Models based on similarity learned embeddings with multi-similarity loss (SLE-MultiSim) exhibit higher average F1-scores and lower variance than alternative approaches. Pairwise controlled manifold approximation (PaCMAP) visualizes high-dimensional spectral similarities in a reduced-dimensional space. Polymers with similar chemical characteristics cluster closely, while microplastics with distinct

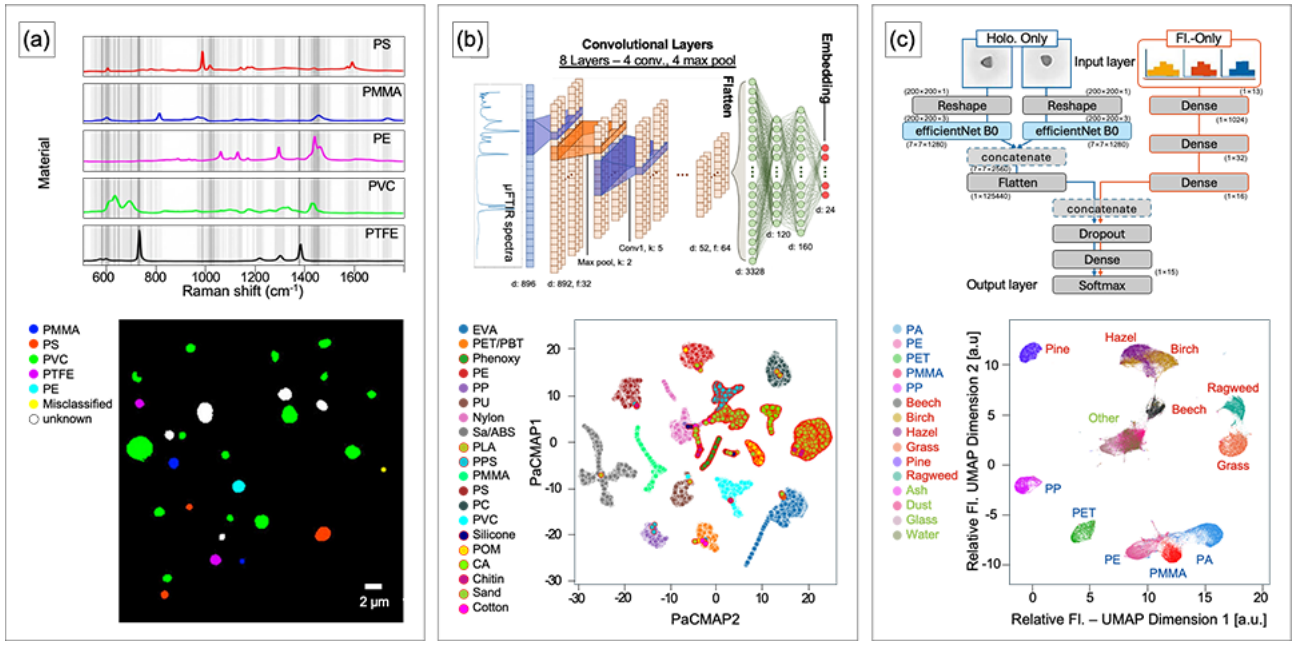

Fig. 7. Machine Learning (ML) assisted analysis and classification of MPs. (a) (top) Visualization of random forest model (gray lines: features of particle categories; darker shade: more important features). (bottom) Particle identification using a random forest model based on Raman spectroscopy. Adapted from Ref. [79]. (b) (top) Architecture of the underlying convolutional neural network (CNN) model. (bottom) Pairwise controlled manifold approximation (PaCMAP) visualization of the embeddings. Adapted from Ref. [83]. (C) (top) Architecture of a ML model (blue: the CNN model using holographic images as input; red: the multilayer perceptron (MLP) model using relative fluorescence spectra; black: concatenated model which using CNN and MLP model). (bottom) Uniform manifold approximation and projection (UMAP) analysis of relative fluorescence spectra. Adapted from Ref. [89].

properties spatially separate.

Additional studies apply 1D CNN models to identify microplastic types [84] or combine ATR-FTIR and Raman spectroscopy prior to 1D CNN analysis [85]. These integrated approaches achieve higher classification accuracy than single-modality spectral analysis. Classification of ATR-FTIR data from real marine samples using k-NN models reports an agreement rate of 90.5% [86].

Studies that integrate ML with EIS primarily employ support vector machine (SVM) models. SVM defines an optimal decision boundary that maximizes the margin between classes. One representative study fills a cylindrical cell with deionized water and flows particles of PP (2, 3, and 4 mm in diameter), PA, PU, POM, PTFE, and glass (4 mm in diameter). EIS measurements generate Nyquist plots under controlled flow conditions. Increasing microplastic concentration reduces the semicircle radius in the Nyquist plot. This feature guides SVM model design and enables the development of a low-cost, field-deployable sensor. The SVM model predicts microplastic material and size an average accuracy of 85% [87]. Other studies compare SVM with k-NN and decision tree models [88]. These analyses perform EIS measurements to obtain Nyquist plots for PET particles (0.5-1, 1-1.5, 1.5-2, and 2-4 mm in size), as well as organic samples (*e.g.*, salmon egg), inert organic samples (*e.g.*, black earth and ground wood), and inorganic samples (*e.g.*, sand). The study evaluates model performance across mixed solutions for each sample set.

ML can also integrate with fluorescence-based microplastic detection [89]. A fluorescence-based platform analyzes airborne microplastics using SwisensPoleno, which an atmospheric monitoring platform that simultaneously records particle images and fluorescence signals (Fig. 7(c)). The dataset includes 15 particle types, comprising 5 microplastics (*i.e.*, PA, PE, PET, PMMA, and PP), 6 pollen species (*i.e.*, Beech, Birch, Hazel, Grass, Pine, and Ragweed), and 4 additional particles (*i.e.*, Ash, Dust, Glass, and Water). Convolutional neural networks train on particle images, while multilayer perceptron (MLP) models train on fluorescence signals. Uniform manifold approximation and projection (UMAP) analyzes fluorescence signal distributions and visualizes clustering in reduced-dimensional space. Fluorescence signals alone enable discrimination at the particle-group level but show limited resolution for individual particle identification within clusters. Combined use of fluorescence and imaging improves classification accuracy to approximately 98%.

Table 1. Comparison of sensing interfaces for micro- and nanoplastic detection.

Interfaces	Key strengths	Sensitivity	Quantification	Specificity (polymer)	Major limitations
Raman spectroscopy	Label-free chemical identification	Moderate	Limited	High	Weak intrinsic signal; Limited sensitivity for nanoplastics; Indirect quantification
SERS	Trace-level detection	Very high	Limited	High	Substrate-dependent signal variability; Reproducibility challenges; Limited standardization
FTIR	Established microplastic analysis	Moderate	Limited	High	Spatial resolution limit for nanoplastics; Water interference
EIS	Simple and low-cost sensing	High (concentration)	Possible (relative)	Low	Lack of chemical specificity; polymer-type ambiguity
Fluorescence	Rapid imaging and counting	High	Limited	Moderate	Requirement for fluorescent staining; Dye nonspecificity; Background fluorescence

3. CONCLUSIONS

Micro- and nanoplastic detection continues to evolve from laboratory-based analytical methods toward integrated sensing platforms designed for complex environmental systems. As summarized in this review, existing techniques—including vibrational spectroscopy, electrochemical impedance analysis, and fluorescence-based sensing—offer complementary strengths in chemical specificity, sensitivity, and operational simplicity. Table 1 compares the major sensing interfaces in terms of sensitivity, quantification capability, and polymer specificity. The comparison highlights that spectroscopic methods offer strong chemical identification but limited quantitative capability, while EIS enables concentration-dependent sensing without intrinsic polymer specificity. Each approach addresses distinct aspects of the micro- and nanoplastics challenge, yet none alone satisfies the requirements for comprehensive environmental monitoring across diverse matrices, particle sizes, and polymer types.

Recent progress highlights a clear transition from single-modality measurements toward platform-level integration. Portable and *in situ* sensing systems increasingly combine selective interfaces, signal amplification strategies, and compact hardware to support real-time analysis outside controlled laboratory settings. These advancements mark an important step toward scalable monitoring frameworks that align with environmental and regulatory demands.

Machine learning further reshapes micro- and nanoplastic sensing by transforming raw spectral, electrical, and optical signals into robust classification and quantification outputs. Data-driven models reduce operator dependence, improve discrimination among chemically similar polymers, and enhance performance in heterogeneous samples. Continued progress in this area depends on standardized datasets, transparent model validation, and closer integration between sensing hardware and analytical algorithms.

Despite these advances, significant technical challenges remain for practical environmental deployment. Real-world samples contain complex mixtures of organic, inorganic, and biological components that interfere with selective detection and reduce measurement reliability. Variations in sample preparation, measurement conditions, and data interpretation across studies further hinder direct comparison and delay the establishment of standardized protocols. In addition, sensor performance under long-term and repeated use remains insufficiently validated, particularly under continuous field operation. These effects complicate conventional spectroscopic analysis, particularly for highly sensitive techniques such as SERS. Machine learning–assisted spectral analysis offers a practical route to address mixed-matrix complexity by extracting discriminative features from overlapping signals and enabling probabilistic classification of coexisting polymers. Integration of SERS with data-driven models therefore provides a promising strategy for reliable microplastic identification in heterogeneous environmental samples.

Therefore, future sensing platforms should prioritize multimodal detection, robustness against environmental variability, long-term operational stability, and sensor reusability. Designs that maintain consistent performance over repeated measurement cycles and extended deployment periods will play a central role in scalable monitoring. Advances in materials design, device engineering, and data analytics collectively support a shift from proof-of-concept

demonstrations toward practical, reliable, and sustainable environmental monitoring of micro- and nanoplastics.

CRediT Authorship Contribution Statement

Seung Yun Kim: Conceptualization, Investigation, Visualization, Writing – original draft. **Rubeen Park:** Conceptualization, Investigation, Visualization, Writing – original draft. **Geumbee Lee:** Conceptualization, Project administration, Supervision, Writing – review and editing.

Declaration of Competing Interest

The authors declare that they have no known competing financial interests or personal relationships that could have appeared to influence the work reported in this paper.

Acknowledgements

This work was supported by Kyungpook National University Research Fund, 2024.

REFERENCES

[1] A. Ter Halle, L. Ladirat, X. Gendre, D. Goudouneche, C. Pusineri, C. Routaboul, et al., Understanding the fragmentation pattern of marine plastic debris, Environ. Sci. Technol. 50 (2016) 5668–5675.
[2] R. Geyer, J.R. Jambeck, K.L. Law, Production, use, and fate of all plastics ever made, Sci. Adv. 3 (2017) e1700782.
[3] K.N. Palansooriya, M.K. Sang, A. El-Naggar, L. Shi, S.X. Chang, J. Sung, et al., Low-density polyethylene microplastics alter chemical properties and microbial communities in agricultural soil, Sci. Rep. 13 (2023) 16276.
[4] A. Ragusa, A. Svelato, C. Santacroce, P. Catalano, V. Notarstefano, O. Carnevali, et al., Plasticenta: First evidence of microplastics in human placenta, Environ. Int. 146 (2021) 106274.
[5] L. Zhu, J. Zhu, R. Zuo, Q. Xu, Y. Qian, L. An, Identification of microplastics in human placenta using laser direct infrared spectroscopy, Sci. Total Environ. 856 (2023) 159060.
[6] G. Lamichhane, A. Acharya, R. Marahatha, B. Modi, R. Paudel, A. Adhikari, et al., Microplastics in environment: global concern, challenges, and controlling measures, Int. J. Environ. Sci. Technol. 20 (2023) 4673–4694.
[7] G.S. Bumbrah, R.M. Sharma, Raman spectroscopy–Basic principle, instrumentation and selected applications for the characterization of drugs of abuse, Egypt. J. Forensic Sci. 6 (2016) 209–215.
[8] N.P. Ivleva, Chemical Analysis of Microplastics and Nanoplastics: Challenges, Advanced Methods, and Perspectives, Chem. Rev. 121 (2021) 11886–11936.
[9] H. De Frond, L.T. Hampton, S. Kotar, K. Gesulga, C. Matuch, W. Lao, et al., Monitoring microplastics in drinking water: An interlaboratory study to inform effective methods for quantifying and characterizing microplastics, Chemosphere 298 (2022) 134282.
[10] R.R. Jones, D.C. Hooper, L. Zhang, D. Wolverson, V.K. Valev, Raman techniques: fundamentals and frontiers, Nanoscale Res. Lett. 14 (2019) 231.
[11] I. Chakraborty, S. Banik, R. Biswas, T. Yamamoto, H. Noothalapati, N. Mazumder, Raman spectroscopy for microplastic detection in water sources: a systematic review, Int. J. Environ. Sci. Technol. 20 (2023) 10435–10448.
[12] M. Perraki, V. Skliros, P. Mecaj, E. Vasileiou, C. Salmas, I. Papanikolaou, et al., Identification of microplastics using μ-Raman spectroscopy in surface and groundwater bodies of SE Attica, Greece, Water 16 (2024) 843.
[13] A.H. Iri, M.H. Shahrah, A.M. Ali, S.A. Qadri, T. Erdem, I.T. Ozdur, et al., Optical detection of microplastics in water, Environ. Sci. Pollut. Res. 28 (2021) 63860–63866.
[14] D.S. Moore, R.J. Scharff, Portable Raman explosives detection, Anal. Bioanal. Chem. 393 (2009) 1571–1578.
[15] J. Jehlička, A. Culka, P. Vandenabeele, H.G. Edwards, Critical evaluation of a handheld Raman spectrometer with near infrared (785 nm) excitation for field identification of minerals, Spectrochim. Acta - A: Mol. Biomol. Spectrosc. 80 (2011) 36–40.
[16] R. Park, W. Jang, P. Faramarzi, D. Oh, G. Lee, H. Lee, et al., Microfluidics-based electrophoretic capture and Raman analysis of micro/nanoplastics, Anal. Chim. Acta (2025) 344829.
[17] R. Gillibert, G. Balakrishnan, Q. Deshoules, M. Tardivel, A. Magazzù, M.G. Donato, et al., Raman tweezers for small microplastics and nanoplastics identification in seawater, Environ. Sci. Technol. 53 (2019) 9003–9013.
[18] X.X. Han, R.S. Rodriguez, C.L. Haynes, Y. Ozaki, B. Zhao, Surface-enhanced Raman spectroscopy, Nat. Rev. Methods Primers 1 (2021) 87.
[19] M. Ku, S. Lee, Y.W. Han, Advanced Strategies for SERS Design as a Next-Generation Biosensing Platform: A Mini Review, J. Sens. Sci. Technol. 34 (2025) 314–323.
[20] S. Choi, S. Lee, M.-K. Kim, E.-S. Yu, Y.-S. Ryu, Challenges and recent analytical advances in micro/nanoplastic detection, Anal. Chem. 96 (2024) 8846–8854.
[21] S.Y. Ding, E.M. You, Z.Q. Tian, M. Moskovits, Electromagnetic theories of surface-enhanced Raman spectroscopy, Chem. Soc. Rev. 46 (2017) 4042–4076.
[22] I. Chaudhry, G. Hu, H. Ye, L. Jensen, Toward Modeling the Complexity of the Chemical Mechanism in SERS, ACS Nano 18 (2024) 208352–20850.
[23] J. Park, S. Lee, H. Lee, S. Han, T.H. Kang, D. Kim, et al., Colloidal Multiscale Assembly via Photothermally Driven Convective Flow for Sensitive In-Solution Plasmonic Detections, Small 18 (2022) 2201075.
[24] E.-S. Yu, E.T. Jeong, S. Lee, I.S. Kim, S. Chung, S. Han, et al., Real-time underwater nanoplastic detection beyond the diffusion limit and low Raman scattering cross-section via electro-photonic tweezers, ACS nano 17 (2022) 2114–2123.
[25] A. Ter Halle, L. Jeanneau, M. Martignac, E. Jardé, B. Pedrono, L. Brach, et al., Nanoplastic in the North Atlantic subtropical gyre, Environ. Sci. Technol. 51 (2017) 13689–13697.
[26] J.Y. Kim, E.H. Koh, J.Y. Yang, C. Mun, S. Lee, H. Lee, et

al., 3D plasmonic gold nanopocket structure for SERS machine learning-based microplastic detection, Adv. Funct. Mater. 34 (2024) 2307584.
[27] C. Rathore, M. Saha, P. Gupta, M. Kumar, A. Naik, J. de Boer, Standardization of micro-FTIR methods and applicability for the detection and identification of microplastics in environmental matrices, Sci. Total Environ. 888 (2023) 164157.
[28] J.-L. Xu, K.V. Thomas, Z. Luo, A.A. Gowen, FTIR and Raman imaging for microplastics analysis: State of the art, challenges and prospects, Trends Anal. Chem. 119 (2019) 115629.
[29] A. Käppler, D. Fischer, S. Oberbeckmann, G. Schernewski, M. Labrenz, K.-J. Eichhorn, B. Voit, Analysis of environmental microplastics by vibrational microspectroscopy: FTIR, Raman or both?, Anal. Bioanal. Chem. 408 (2016) 8377–8391.
[30] A.S. Tagg, M. Sapp, J.P. Harrison, C.J. Sinclair, E. Bradley, Y. Ju-Nam, et al., Microplastic monitoring at different stages in a wastewater treatment plant using reflectance micro-FTIR imaging, Front. Environ. Sci. 8 (2020) 145.
[31] X. Fan, W. Zheng, D.J. Singh, Light scattering and surface plasmons on small spherical particles, Light: Sci. Appl. 3 (2014) e179.
[32] P. Bruździak, Vapor correction of FTIR spectra–A simple automatic least squares approach, Spectrochim. Acta A Mol. Biomol. Spectrosc. 223 (2019) 117373.
[33] D. Schymanski, B.E. Oßmann, N. Benismail, K. Boukerma, G. Dallmann, E. Von der Esch, et al., Analysis of microplastics in drinking water and other clean water samples with micro-Raman and micro-infrared spectroscopy: minimum requirements and best practice guidelines, Anal. Bioanal. Chem. 413 (2021) 5969–5994.
[34] J. Yang, Y.-P. Xu, X.-L. Chu, Quantitative analysis of plastic blends based on virtual mid-infrared spectroscopy combined with chemometric methods, Talanta 292 (2025) 128006.
[35] S.-F. Pang, J. Wang, Y. Zhang, C.-B. Leng, Y.-H. Zhang, A new method for estimating the extinction efficiency of polystyrene microsphere by micro-FTIR spectroscopy, Spectrochim. Acta A 181 (2017) 249–253.
[36] F. Corami, B. Rosso, B. Bravo, A. Gambaro, C. Barbante, A novel method for purification, quantitative analysis and characterization of microplastic fibers using Micro-FTIR, Chemosphere 238 (2020) 124564.
[37] S. Zhang, W. Zhang, M. Ju, L. Qu, X. Chu, C. Huo, et al., Distribution characteristics of microplastics in surface and subsurface Antarctic seawater, Sci. Total Environ. 838 (2022) 156051.
[38] A.R. de Carvalho, O. Mathieu, M. Thevenot, P. Amiotte-Suchet, X. Bertrand, J.-C. Beugnot, et al., Determination of polystyrene microplastic in soil by pyrolysis–gas chromatography–mass spectrometry (pyr-GC-MS), Anal. Lett. 57 (2024) 1576–1594.
[39] T. Ishimura, I. Iwai, K. Matsui, M. Mattonai, A. Watanabe, W. Robberson, et al., Qualitative and quantitative analysis of mixtures of microplastics in the presence of calcium carbonate by pyrolysis-GC/MS, J. Anal. Appl. Pyrolysis 157 (2021) 105188.
[40] T.T. Dang, E. Sogut, I. Uysal-Unalan, M. Corredig, Quantification of polystyrene microplastics in water, milk, and coffee using thermogravimetry coupled with fourier transform infrared spectroscopy (TGA-FTIR), Chemosphere 368 (2024) 143777.
[41] J. Yu, P. Wang, F. Ni, D. Wu, Q. Zhao, Y. Zhou, Characterization of microplastics in environment by thermal gravimetric analysis coupled with Foureier transform infrared spectroscopy, Mar. Pollut. Bull. 145 (2019) 153–160.
[42] F. Blancho, M. Davranche, H.E. Hadri, B. Grassl, J. Gigault, Nanoplastics identification in complex environmental matrices: Strategies for polystyrene and polypropylene, Environ. Technol. 55 (2021) 8753–8759.
[43] B.-Y. Chang, S.-M. Park, Electrochemical impedance spectroscopy, Annu. Rev. Anal. Chem. 3 (2010) 207–229.
[44] A.C. Lazanas, M.I. Prodromidis, Electrochemical impedance spectroscopy- a tutorial, ACS Meas. Sci. Au 3 (2023) 162–193.
[45] W. Choi, H.C. Shin, J.M. Kim, J.Y. Choi, W.S. Yoon, Modeling and Applications of Electrochemical Impedance Spectroscopy (EIS) for Lithium-ion Batteries, J. Electrochem. Sci. Technol. 11 (2020) 1–13.
[46] D. Preethichandra, P. Sonar, Electrochemical impedance spectroscopy and its applications in sensor development and measuring battery performance, IEEE Sens. J. 22 (2021) 10152–10162.
[47] W. Hu, X. Lv, Advanced electrochemical and sensor technologies in gastroenterology: Applications of EIS, organ-on-a-chip, and ingestible/wearable devices in chronic disease diagnosis and monitoring, Int. J. Electrochem. Sci. (2025) 101178.
[48] J.A. Ribeiro, P.A.S. Jorge, Applications of electrochemical impedance spectroscopy in disease diagnosis-A review, Sens. Actuators Rep. 8 (2024) 100205.
[49] R. Maallah, A. Moutcine, C. Laghlimi, M. Smaini, A. Chtaini, Electrochemical bio-sensor for degradation of phenol in the environment, Sens. Bio-Sens. Res. 24 (2019) 100279.
[50] C. Li, Y. Ma, Y. Li, F. Wang, EIS monitoring study of atmospheric corrosion under variable relative humidity, Corros. Sci. 52 (2010) 3677–3686.
[51] O. Kanoun, A.Y. Kallel, H. Nouri, B. Ben Atitallah, D. Haddad, Z. Hu, et al., Impedance Spectroscopy: Applications, Advances and Future Trends, IEEE Instrum. Meas. Mag. 25 (2022) 11–21.
[52] A. Motalebizadeh, S. Fardindoost, M. Hoorfar, Selective on-site detection and quantification of polystyrene microplastics in water using fluorescence-tagged peptides and electrochemical impedance spectroscopy, J. Hazard. Mater. 480 (2024) 136004.
[53] A.B. Silva, A.S. Bastos, C.I.L. Justino, J.A.P. da Costa, A.C. Duarte, T.A.P. Rocha-Santos, Microplastics in the environment: Challenges in analytical chemistry A review, Anal. Chim. Acta 1017 (2018) 1–19.
[54] C.Q. Peng, Y.S. Thio, R.A. Gerhardt, Effect of Precursor-Layer Surface Charge on the Layer-by-Layer Assembly of

Polyelectrolyte/Nanoparticle Multilayers, Langmuir 28 (2012) 84–91.
[55] S. Martic, M. Tabobondung, S. Gao, T. Lewis, Emerging electrochemical tools for microplastics remediation and sensing, Front. Sens. 3 (2022) 958633.
[56] H. Du, G. Chen, J. Wang, Highly selective electrochemical impedance spectroscopy-based graphene electrode for rapid detection of microplastics, Sci. Total Environ. 862 (2023) 160873.
[57] B.C. Colson, A.P.M. Michel, Flow-Through Quantification of Microplastics Using Impedance Spectroscopy, Acs Sens. 6 (2021) 238–244.
[58] M. Urso, M. Ussia, F. Novotny, M. Pumera, Trapping and detecting nanoplastics by MXene-derived oxide microrobots, Nat. Commun. 13 (2022) 3573.
[59] W. Gongi, H. Touzi, I. Sadly, H. Ben Ouada, O. Tamarin, H. Ben Ouada, A Novel Impedimetric Sensor Based on Cyanobacterial Extracellular Polymeric Substances for Microplastics Detection, J. Polym. Environ. 30 (2022) 4738–4748.
[60] Y.K. Song, S.H. Hong, M. Jang, G.M. Han, M. Rani, J. Lee, et al., A comparison of microscopic and spectroscopic identification methods for analysis of microplastics in environmental samples, Mar. Pollut. Bull. 93 (2015) 202–209.
[61] S. Mariano, S. Tacconi, M. Fidaleo, M. Rossi, L. Dini, Micro and Nanoplastics Identification: Classic Methods and Innovative Detection Techniques, Front. Toxicol. 3 (2021) 636640.
[62] C.H. Chin, S.H. Lin, Theoretical investigations of absorption and fluorescence spectra of protonated pyrene, Phys. Chem. Chem. Phys. 18 (2016) 14569–14579.
[63] S.A. Mason, V.G. Welch, J. Neratko, Synthetic Polymer Contamination in Bottled Water, Front. Chem. 6 (2018) 407.
[64] L.L. Lv, J.H. Qu, Z.H. Yu, D.H. Chen, C.X. Zhou, P.Z. Hong, et al., A simple method for detecting and quantifying microplastics utilizing fluorescent dyes - Safranine T, fluorescein isophosphate, Nile red based on thermal expansion and contraction property, Environ. Pollut. 255 (2019) 113283.
[65] H. Aoki, M. Torimura, H. Habe, Spectroscopic Investigation of Increased Fluorescent Intensity of Fluorescent Dyes When Adsorbed onto Polystyrene Microparticles, Anal. Sci. 37 (2021) 773–779.
[66] N. Klippel, G.G. Jung, G. Kickelbick, Hybrid inorganic-organic fluorescent silica nanoparticles-influence of dye binding modes on dye leaching, J. Sol-Gel Sci. Technol. 107 (2023) 2–19.
[67] H.L. Du, Y.S. Zhang, H.R. Jiang, H. Wang, Adsorption of rhodamine B on polyvinyl chloride, polystyrene, and polyethylene terephthalate microplastics in aqueous environments, Environ. Technol. Innov. 27 (2022) 102495.
[68] A.S. Kristoffersen, S.R. Erga, B. Hamre, O. Frette, Testing Fluorescence Lifetime Standards using Two-Photon Excitation and Time-Domain Instrumentation: Rhodamine B, Coumarin 6 and Lucifer Yellow, J. Fluoresc. 24 (2014) 1015–1024.
[69] H.Y. Tong, Q.Y. Jiang, X.C. Zhong, X.S. Hu, Rhodamine B dye staining for visualizing microplastics in laboratory-based studies, Environ. Sci. Pollut. Res. 28 (2021) 4209–4215.
[70] T. Maes, R. Jessop, N. Wellner, K. Haupt, A.G. Mayes, A rapid-screening approach to detect and quantify microplastics based on fluorescent tagging with Nile Red, Sci. Rep. 7 (2017) 44501.
[71] S.H. Han, D.G. Kim, H.Y. Jung, S.H. Kim, Study on Real Time Sensor Monitoring Systems Based on Pulsed Laser for Microplastic Detection in Tap Water, J. Sens. Sci. Technol. 28 (2019) 294–298.
[72] S. Sirimak, A. Sappat, J. Thangphatthanarungruang, N. Watthanawisuth, R. Keawkanha, T. Lomas, et al., Innovative portable microplastic detector using a continuous flow technique with fluorescence Nile red-graphene oxide, Int. J. Environ. Sci. Technol. 22 (2025) 12831–12842.
[73] J. Leonard, H.C. Koydemir, V.S. Koutnik, D. Tseng, A. Ozcan, S.K. Mohanty, Smartphone-enabled rapid quantification of microplastics, J. Hazard. Mater. Lett. 3 (2022) 100052.
[74] C.Q.V. Costa, J. Cruz, J. Martins, M.A.A. Teodósio, S. Jockusch, V. Ramamurthy, et al., Fluorescence sensing of microplastics on surfaces, Environ. Chem. Lett. 19 (2021) 1797–1802.
[75] T. Stanton, M. Johnson, P. Nathanail, R.L. Gomes, T. Needham, A. Burson, Exploring the Efficacy of Nile Red in Microplastic Quantification: A Costaining Approach, Environ. Sci. Tech. Lett. 6 (2019) 606–611.
[76] J.I. García-Plazaola, B. Fernández-Marín, S.O. Duke, A. Hernándeza, F. López-Arbeloa, J.M. Becerril, Autofluorescence: Biological functions and technical applications, Plant Sci. 236 (2015) 136–145.
[77] R.-C. Chen, C. Dewi, S.-W. Huang, R.E. Caraka, Selecting critical features for data classification based on machine learning methods, J. Big Data 7 (2020) 52.
[78] F. Muharemi, D. Logofătu, F. Leon, Machine learning approaches for anomaly detection of water quality on a real-world data set, J. Inf. Telecommun. 3 (2019) 294–307.
[79] L. Xie, S. Luo, Y. Liu, X. Ruan, K. Gong, Q. Ge, et al., Automatic identification of individual nanoplastics by Raman spectroscopy based on machine learning, Environ. Sci. Technol. 57 (2023) 18203–18214.
[80] C. Fang, Y. Luo, R. Naidu, Advancements in Raman imaging for nanoplastic analysis: Challenges, algorithms and future Perspectives, Anal. Chim. Acta 1290 (2024) 342069.
[81] Y. Luo, W. Su, M.F. Rabbi, Q. Wan, D. Xu, Z. Wang, et al., Quantitative analysis of microplastics in water environments based on Raman spectroscopy and convolutional neural network, Sci. Total Environ. 926 (2024) 171925.
[82] U.E. Hogan, H.B. Voss, B. Lei, R.D. Smith, Integrating C–H Information to Improve Machine Learning Classification Models for Microplastic Identification from Raman Spectra, Anal. Chem. 97 (2025) 2214–2222.
[83] J.A. Smolen, G.E. Moore, N.D. Perez, K.L. Wooley,

Adaptable microplastic classification using similarity learning on μFTIR spectra collected from μFTIR focal plane array imaging, Proc. Natl. Acad. Sci. U.S.A. 122 (2025) e2509745122.
[84] E. Choi, Y. Choi, H. Lee, J.W. Kim, H.B. Oh, Development of a machine-learning model for microplastic analysis in an FT-IR microscopy image, Bull. Korean Chem. Soc. 45 (2024) 472–481.
[85] H. Li, S. Xu, J. Teng, X. Jiang, H. Zhang, Y. Qin, et al., Deep learning assisted ATR-FTIR and Raman spectroscopy fusion technology for microplastic identification, Microchem. J. 212 (2025) 113224.
[86] M. Kedzierski, M. Falcou-Préfol, M.E. Kerros, M. Henry, M.L. Pedrotti, S. Bruzaud, A machine learning algorithm for high throughput identification of FTIR spectra: application on microplastics collected in the Mediterranean Sea, Chemosphere 234 (2019) 242–251.
[87] V. Meiler, J. Pfeiffer, L. Bifano, C. Kandlbinder-Paret, G. Fischerauer, Approaches to detect microplastics in water using electrical impedance measurements and support vector machines, IEEE Sens. J. 23 (2023) 4863–4872.
[88] J. Sarmiento, M. Anaya, D. Tibaduiza, Microplastic identification using impedance spectroscopy and machine learning algorithms, Int. J. Distrib. Sens. Netw. 2024 (2024) 5298635.
[89] N.D. Beres, J. Burkart, E. Graf, Y. Zeder, L.A. Dailey, B. Weinzierl, Merging holography, fluorescence, and machine learning for in situ, continuous characterization and classification of airborne microplastics, EGUsphere 2023 (2023) 1–31.

Seung Yun Kim is currently a master's candidate under the supervision of Prof. Geumbee Lee of the School of Chemical Engineering and Applied Chemistry at Kyungpook National University (KNU). He received his B.S. degree in Department of Chemical Engineering at KNU in 2025. His research focuses on biodegradable/bioresorbable and implantable devices for healthcare and environmental systems.

Rubeen Park is currently a Ph.D. candidate under the supervision of Prof. Geumbee Lee of the School of Chemical Engineering and Applied Chemistry at Kyungpook National University. She received her B.S. degree in Department of Chemical Engineering at Yeungnam University in 2023. Her research focuses on electrical/electrochemical environmental sensors for microplastic detection.

Geumbee Lee is an Assistant Professor in the School of Chemical Engineering and Applied Chemistry at Kyungpook National University. She received her degree in Nano-Bio-Information-Technology from Korea University in 2019. She then moved to the Northwestern University as a postdoctoral fellow in the Querrey Simpson Institute for Bioelectronics. Her research interests include eco/biodegradable, resorbable and compatible electronic materials, devices, and applications. For more information, please visit the website: http://bell.knu.ac.kr